Gadau Journal of Pure and Allied Sciences
Gadau J Pure Alli Sci, 3(2): 46-53 (2024)
ISSN: 2955-1722
DOI: https://doi.org/10.54117/gjpas.v3i2.152

G_0W_0 Calculations of optoelectronic properties of Graphene/hBN for Solar cells and near infrared Photodetector

Dauda Abubakar[1], Musa Muhammad Salihu[1], Abdullahi Lawal[2]*, Musa Bello[3], Ahmed Musa Kona[3] and Sadiq Abubakar Dalhatu[4]

[1]Department of Physics, Faculty of Science, Sa'adu Zungur University Gadau, Bauchi State, Nigeria.
[2]Department of Physics, Ahmadu Bello University, Zaria, Kaduna State, Nigeria.
[3]Department of Physics, Federal University of Education, Zaria, Kaduna State, Nigeria.
[4]Federal University of Health Sciences Azare, Bauchi State, Nigeria.

**Correspondence: abdullahikubau@yahoo.com; +2347033860054*

Abstract

It is known that low optical absorption in graphene-based devices can be dramatically improved. However, integrating hexagonal boron nitride (hBN) with graphene in a heterostructure appears to be a promising approach to open the band gap in graphene in order to overcome the low absorption behavior in graphene-based devise for optoelectronic applications. Hence, to expose the hidden potential of hBN heterostructure, detailed knowledge of its electronic properties are needed. In this paper, electronic properties of hBN/graphene heterostructure are performing by highly accurate first-principles many-body perturbation theory. The calculated G_0W_0 band gap of hBN sheet was found to be 6.09 eV and this value is in good agreement with experimental value of 6 eV. For the heterostructure the calculated band gaps of hBN/graphene by varying the interlayer distance from 1.5 to 3.5 Å was found to be 1.76, 1.70, 0.84, 0.22 0.04 eV for interlayer distance of 1.5, 2.0, 2.5, 3.0 and 3.5 eV. The energy analysis of hBN/graphene heterostructure reveals that the most stable configuration is the one in which the either B or N atom of hBN facing to graphene is above the hole center of graphene. More attractively, strong absorption within visible light wavelengths in hBN/graphene sheets suggest that the heterostructure is a promising candidate for solar cells applications.

Article History
Received: 11/07/2024
Accepted: 29/11/2024
Published: 31/12/2024

Keywords:
Graphene, hBN, DFT, G_0W_0, Electron-electron interaction, Photodetector.

How to cite this paper: Dauda A., Musa M. S., Abdullahi L., Musa B., Ahmed M. K., and Sadiq A. D. (2024). G_0W_0 Calculations of optoelectronic properties of Graphene/hBN for Solar cells and near infrared Photodetector. *Gadau J Pure Alli Sci, 3(2): 46-53.* https://doi.org/10.54117/gjpas.v3i2.152

1.0 Introduction

Graphene as the last member of carbon set has received a lot of attention since it was isolated experimentally via mechanical exfoliations method in 2004 by Novoselov et al., (Novoselov *et al*., 2004). A novel graphene has hexagonal structure with exceptional characteristics such as high carrier mobility, Dirac-cone, chiral transport, excellent conductivity and so on. These characters make graphene a promising material for super capacitors (Liu *et al*., 2012), catalysis (Ahmed *et al*., 2021) applications and so on. Absence of band gap, low optical absorption limited its application as graphene-based science and technology (Itas, Suleiman, Ndikilar, Lawal, Razali, Khandaker, et al., 2023; Lawal *et al*., 2019; Santra *et al*., 2024). Generally, the most important limitation of utilizing graphene for optoelectronic application is its gapless nature which result to poor optical absorption. Therefore, regards to applications opening fundamental energy gap is crucial for electronic devices. Thus, tuning the fundamental band gap of graphene has triggered enormous interest in fabricating and designing electronic devices with high performance. Different approaches

have been developed to overcome this problem such as graphene nanowire (Liu *et al*., 2017), adsorbing molecules on the surface of graphene (Ersan *et al.*, 2017), graphene nanoribbons (Chen *et al*., 2006), substituting carbon atoms with heteroatoms (Quílez-Bermejo *et al*., 2020), epitaxial growth of graphene on substrate and so on (Jariwala et al., 2011; Wang et al., 2021). However, such approaches have difficulties in fabrication process and could not guarantee better performance due to the degradation of carrier mobility in graphene. On the other hand, integrating other two dimensional (2D) semiconductor materials with graphene appears to be the most promising method (Das *et al*., 2019). In this paper, hexagonal boron nitride (h-BN is chosen as 2D material because it has smooth surface and it is chemically and thermally stable. The lattice parameters of h-BN is similar to that of graphene with strong covalent bond between B and N atoms together and the layers are bonded by van der Waals forces (Yang *et al*., 2024). The fundamental band gap of h-BN was found experimentally to be about 4.5 to 6 eV (Solozhenko et al., 2001; Wang *et al*., 2019; Watanabe *et al*., 2004) and this makes it an excellent insulator. Therefore, for the optimal operation of this heterostructure for device applications, accurate measurements of the structural and electronic properties are needed. Computational ab initio methodologies based on Density Functional Theory (DFT) are intensely used by the theoretical researchers to solve the complex problems (Lawal *et al*., 2017a, 2017b; Radzwan *et al*., 2018). It was found that ab-initio methods based on standard density functional theory (DFT) provide useful ltools for the prediction and characterization of the ground-state properties of the materials such as atomic configuration and total energies (Idris *et al*., 2021; Idris *et al*., 2020; Yusuf et al., 2024). However, bandgap energy is usually underestimated within such methods particularly based on standard LDA or GGA. The underestimation of the energy band gap in DFT approach is due to approximations used to estimate the exchange-correlation functional part of energy/potential, resulting in the failure to predict the right value of the quasiparticle eigenenergies (Luo *et al*., 2012). hence, to overcome this discrepancy between DFT calculations and experimental results, self-energy correction to the quasiparticle (QP) energy is essential (Harsha *et al*., 2024; Lawal, Taura, *et al*., 2022). Consequently, one-particle Green's function based on many-body perturbation theory (MBPT) within non-self-consistent GW approach (one-shot G0W0 approximation) is the most reliable and one of the cheapest methods for computing quasiparticle (QP) bandgap closer to experimental measurements (Aga *et al*., 2023; Lawal, Bello, *et al*., 2022). In this work, calculations of structural parameters are performed within DFT framework as implemented in Quantum Espresso simulation package (Giannozzi *et al*., 2009). Electronic and optical properties are calculated using many-body perturbation theory (MBPT) by mean of G0W0 approximation.

2. 0 Computational Details

In this study all calculations have been performed with fully optimized atomic internal coordinates and lattice parameters for full first-principles philosophy, meaning that all the calculations are from first-principles without adjusting any parameters. In general, all ground state calculations are performed based on plane wave basis set DFT code, Quantum Espresso. Norm-conserving pseudopotentials generated via Rappe-Rabe-Kaxiras-Joannopoulos (RRKJ) technique (Giannozzi, 2010) were used to model the interactions between valence electrons and ionic core potential of C, B and N. For structural relaxation, the electron-electron are treated with generalized gradient approximation (GGA) in the form of Perdew–Berke–Erzndof (PBE) functionals and local density approximation (LDA). In addition to the semi-local GGA and LDA, we implemented a vdW-DF approach for the exchange-correlation functional to take into account the effect of van der Waals (vdW) interaction. All the lattice parameters were relaxed until Hellmann-Feynman force acting on each ion is less than 5×10^{-5} eV/Å and the convergence threshold energy used was 10^{-9} eV for self-consistent calculations. The plane wave kinetic energy for structural relaxation set to be 50 Ry with a charge density of 475 Ry. The effect of spin-orbit coupling (SOC) is treated self-consistently with full relativistic norm-conserving pseudopotentials of standard solid-state pseudopotential library of Dal Corso et al (Dal Corso et al., 1993). . For electronic properties calculations of the graphene/hBN 4×4 supercell structure containing 32 atoms of graphene and 32 atoms of atoms of hBN. The electron-electron and van der Waals effects were treated with generalized gradient approximation (GGA) in the form of Perdew–Berke–Erzndof (PBE) functionals and vdW approach [134]. Plane-wave kinetic energy cut-offs of 45 Ry and charge density of 350 Ry was found to be sufficient for calculating electronic band structures. The irreducible Brillouin zone was sampled with a set of 10×10×1 Monkhorst-Pack grid to generate k-points and denser value of 16×16×1 was used for the density of states using a technique known as Hermite-Gaussian smearing. To avoid unwanted interactions between the nearest slabs a large vacuum layer of 25 Å was used so that periodic images and the layer can be treated independently. The separation distance between hBN as photoactive material and graphene surface as the electrode is measured. We vary the distance between graphene and hBN to be from 1.5 to 3.5 Å respectively. The equation used for computing the binding energy can be written as:

$$\text{Binding energy} = E_{grap/hBN} - \left(E_{hBN} + E_{grap}\right) \quad (1)$$

Quasiparticle (QP) band structure is calculated by GW approximation for the self-energy operator Σ.

Specifically, frequency dependence of the dielectric matrix were treated by single one shot G_0W_0 approximation via Godby-Needs plasmon pole model (Godby & Needs, 1989a, 1989b). All many-body perturbation theory (MBPT) calculations were performed via Yambo package (Marini *et al*., 2009).

3.0 Results and Discussion

3.1 Convergence Test Results of graphene and hBN

In order to get a well-converged total energy, there is need to test all other parameters relatively on a convergence scale to ensure that convergence is achieved consistently. Because, a "numerically converged" calculation usually gives an approximate solution that is often considered as the accurate solution of the mathematical equation given by DFT with exact exchange-correlation functional, even though the exact functional is not known. Therefore, understanding convergences with respect to plane-wave kinetic energy cutoff and *k*-points mesh is very essential. The results presented in Figure 2 represent the convergence test with respect to plane wave kinetic energy cut-off and k-points mesh for graphene and hBN single layers. Figure 2 and 3 displayed the results of converging test of graphene and hBN sheets. Figure 2(a) and 3(a) shows that the total energy changes significantly with the kinetic energy cut-off, until at some energy cut-off where it turns out to be almost stable. In all the two cases, the kinetic energy cut-off increases from 10Ry to 30Ry and becomes stable at 30Ry. It indicates that the total energy remains constant without any further increases in the kinetic energy cut-off from 30Ry. This shows a well-converged energy cut-off. That is the reason 40Ry was used as the plane wave basis set for the kinetic energy cut-off of all the two cases that is in graphene and hBN.

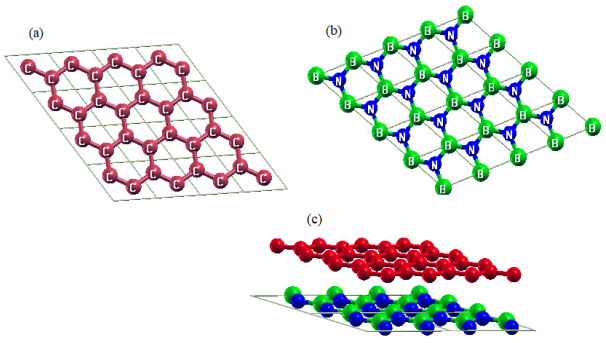

Figure 1: Crystal structure of (a) Graphene (b) hBN (c) Graphene/hBN heterostructure

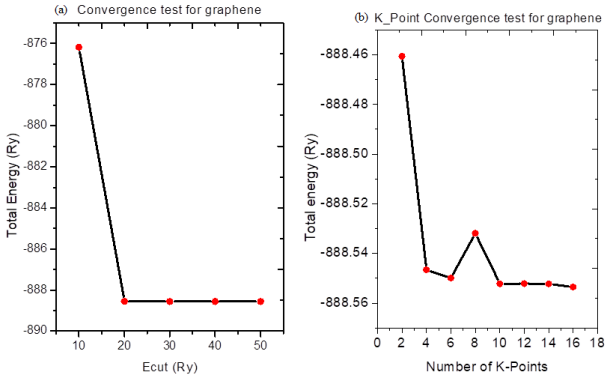

Figure 2: (a) The convergence of total energy with respect to the kinetic energy cut-off for graphene (b) The convergence of the total energy with respect to the k-points grids for grapheme.

However, Figures 2(b) and 3 (b), shows that the total energy is independent of the number of *k*-points at a certain point, showing a well converged value. The energy changes considerably as the number of *k*-point changed, up to a particular point where it remains unchanged. In all the twoe cases, the total energy increases from 2×2×1 to 8×8×1 k-point grids and become stable at 10×10×1.Monkhorst and Pack method of selecting *k*-points is widely used in most DFT calculations (Monkhorst & Pack, 1976). Most of the DFT codes provide ways of selecting *k*-points using Monkhorst and Pack method. One of the basic ideas used in this method is to specify the number of *k*-points that are to be used in each direction in reciprocal space. In this work, the 12×12×1 *k* points were adopted for all calculations.

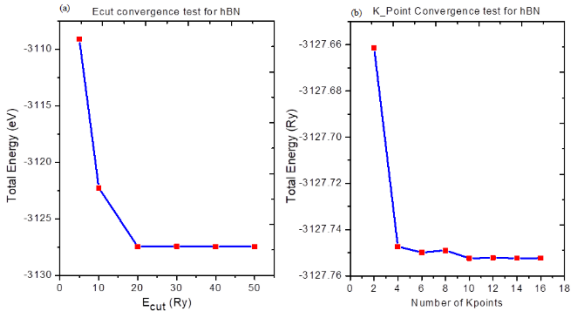

Figure 3: (a) The convergence of total energy with respect to the kinetic energy cut-off for hBN (b)

The convergence of the total energy with respect to the k-points grids for hBN.

3.2 **Band structure of graphene and hBN sheets**

The calculated electronic properties of graphene and hBN are computed within PBE approximation based on DFT and GW within G_0W_0 approximation. G_0W_0 approximation is used in this work in order to produce a reliable and more accurate energy gap. For band structure calculations the selected high symmetry points are K(1/3,2/3,0), Γ(0,0,0) and M(0,1/2,0) respectively. The energy band gap in graphene was found to be zero as shown in Figure 3 (a) and this value is in good agreement with previous theoretical and experimental work (Huang et al., 2017; Medeiros et al., 2014; Xu et al., 2021). In graphene band structure plot the conduction band and the valence band intersect at one point, which is called the Dirac point. In the case of hexagonal boron nitrogen (hBN) sheet the calculated band gap with PBE potential was found to be 3.61 eV and this value is consistent with previous first principle results (Huang & Lee, 2012; Zhao et al., 2012). However, the value is smaller than the experimental result of 6 eV (Shi et al., 2010; Song et al., 2010) due to the approximation used in the exchange correlation functionals. However, to resolve the above-mentioned issues that is inconsistency in bandgap value between standard DFT calculations and experiment, we further performed G_0W_0 calculation. The GW approximation is known to be accurate to about 0.1 eV (Hybertsen & Louie, 1984), inclusion of GW approximation brings the band-gap of pure hBN sheet to value to 6.09 eV and this value is in agreement with experimental value of 6 eV (Shi et al., 2010; Song et al., 2010).

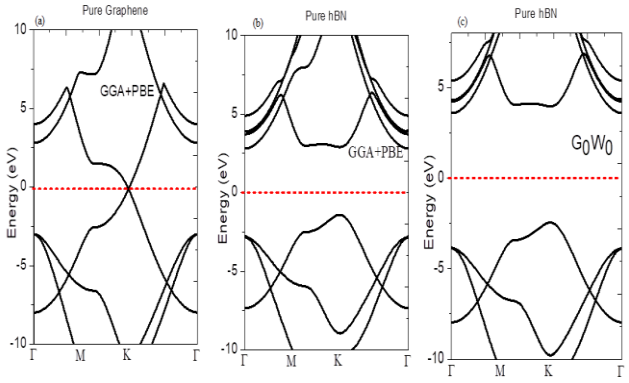

Figure 4: Electronic band structure of (a) graphene with GGA+PBE (b) hBN with GGA+PBE (c) hBN with G_0W_0

3.3 Band structure of hBN/graphene heterostructure

Generally, Interfacing materials with different topological orders have received great attention for finding new physical states for versatile of applications that affect our lives (Mondal & Pati, 2012). Furthermore, among the aforesaid methods, the interface approach is believed particularly a promising way to render practical applications into a reality where exploration on the nature of the adsorbate-substrate is essential before fabricating the system into reality (Margine et al., 2008). The key achievement in assessing the interaction and describing the desired properties majorly depends on the use of theoretical methods instead of experimental works without grasping the prior knowledge in advance. In this context, theoretical methods of quantum mechanical techniques based on G_0W_0 approximations are favored in producing reliable results especially in characterizing electronic properties of adsorbate-substrate. Interfacing hBN sheet with other materials such as graphene can provide an exciting platform to explore phenomena of Dirac fermions at the interfaces. Graphene provides an excellent transport channel for optoelectronic application while strong light absorption in hBN sheet can be used to overcome the 2.3% absorption in graphene. Therefore, combining graphene and hBN can offer some important effects without degrading the properties of graphene and hBN. Furthermore, a conventional unit cell of hBN sheet has hexagonal crystal structure similar to graphene. The unique properties of both graphene and hBN motivate us to explore what will happen in hBN/graphene by altering the distance between hBN sheet and graphene sheet. Firstly, in order to obtain the most stacking pattern and stable configuration, an energetic investigation has been performed. In the stacking pattern, three different configurations are considered. We start with the initial stacking pattern: P, with the position of either B or N atom facing the hollow centre of graphene's hexagonal lattice; follow by Q, eithe N or B atom facing directly above carbon atom and lastly R, the position of either B or N atom facing to graphene above the middle position of the two adjacent carbon atoms. In order to tune and find the flexibility gap of hBN/graphene, the separation distance between the hBN and graphene was varied from 1.5 Å to 3.5 Å. Figure 4 shows the energy analysis of the three configurations. For all the three configurations the total energy decreases with increasing interlayer distance between hBN and graphene. Therefore, a large value of the interlayer distance between hBN and graphene show very weak bonding. As shown in Figure 5, the energy analysis reveals that themost stable configuration is the one in which the either B or N atoms facing to graphene is above the hole centre of graphene's hexagonal lattice.

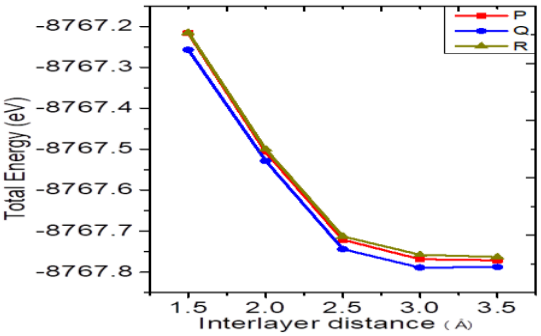

Figure 5: Calculated energy curve of hBN/graphene as a function of interlayer distance for all the three configurations.

Since first-principles many-body paturbation theory calculations is too expensive, the main focus should be on the more stable structure. Figure 6 and 7 show calculated band structure of hBN/graphene by varying the interlayer distance from 1.5 to 3.5 Å respectively. Referring to Figure 4.4, hybridization between hBN sheet and graphene sheet at smaller interlayer distance resulted in large energy gap of 1.76, 1.70 and 0.84 eV at interlayer distance of d = 1.5, 2.0 and 2.5 Å respectively, indicating that at these distance hBN/graphene can be use for solar cell application because the band gap value is within the visible light wavelenghts. The large energy gap in smaller distance between hBN and graphene is due to very strong hybridization between graphene and hBN. However, the large energy gap is then started reducing drastically from d = 3.0 Å as can be seen in Figure 7. Figure 7 shows that at d = 3.5 Å the interaction between graphene and is a very weak which leads to the closure of graphene Dirac states because the energy gap was just 0.04 eV. This indicates that the interfacing distance plays a vital role in providing the different strength of interlayer interactions between the adsorbate and the substrate surface; hBN and graphene, which in this case has led to the increase of the energy gap at small interfacing distance. These findings gave a tremendous impact since a noticeable energy gap of the graphene is created in the presence of hBN sheet. This consequently leads the pathways of assembling a variety of applications with the semiconductor-like properties of graphene.

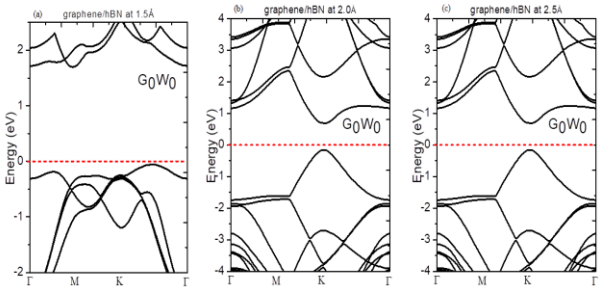

Figure 6: Band structures of graphene on top hBN at (a) 1.5 Å (b) 1.5 Å and (c) 3.5 Å interface

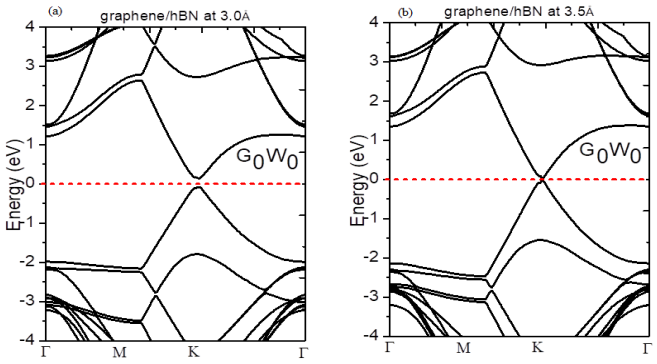

Figure 7: Band structures of graphene on top hBN at (a) 3.0 Å (b) 3.5 Å interface.

3.4 Optical Properties

The study of the optical properties of a material is crucial to get insight view about its characteristics for applications in the optoelectronic system and devices. From the comprehensive literature review, it is found that the exploration of the optical features relating to hBN/graphene are scarcely done. To complete the study on optoelectronic properties, in addition to the electronic properties, in this section, a comprehensive study is presented on the optical absorption of the pure hBN sheet and hBN/graphene by highly accurate method using random phase approximation (RPA) based on G_0W_0 (G_0W_0+RPA), which include electron-electron (e-e) interactions. Although optical properties calculation via G_0W_0+RPA is computationally expensive, it provides accurate description of absorption spectra. Several studies have shown that inclusion of e-e interactions gives accurate description of the optical spectra (Escudero et al., 2017; Itas, Razali, et al., 2023; Itas, Suleiman, Ndikilar, Lawal, Razali, Ullah, et al., 2023; Körbel et al., 2016; Rohlfing & Louie, 2000). The optical parameter considered in this paper is imaginary $\varepsilon_2(\omega)$ which correspond to optical absorptions. The imaginary part $\varepsilon_2(\omega)$ of frequency dependent of the dielectric function relates to the manner by which light is absorbed by the medium (LAWAL, 2017; Lawal et al., 2017a). The obtained imaginary part of frequency-dependent dielectric function of pure hBN sheet and hBN/graphene at interlayer distance of 2.0 Å using G_0W_0+RPA method are displayed in Figure 8, respectively. For hBN sheet the first critical point sometimes called edge of optical absorption (optical gap) occurred at about 6.09 eV, this value correspond to quasi-particle band gap (G_0W_0 band gap). The calculated optical gap of hBN sheet is in good

agreement with experimental data of 6.0 eV. This point split the valence band maximum and conduction band minimum. For hBN/graphene sheets the first absorption peak which correspond to the first bound exciton located at 1.7 eV. Conparing the optical absoption spectra, absorption in hBN/graphene is almost eight times that of pure hBN sheet. Optical gap of 1.7 eV and strong absorption within visible light waveleghts in hBN/graphene sheets suggest that the heterostruture consider in this thesis is a promising candidate for solar cells applications.

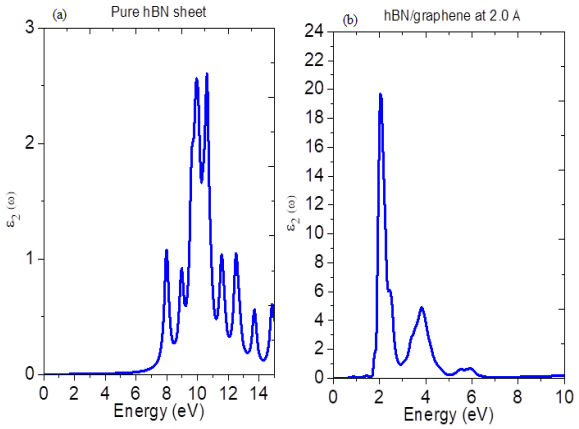

Figure 8: The imaginary part of frequeny-dependent dielectric function of: (a) hBN sheet (b) hBN/graphene hetrostructure.

5.0 Conclusion

In this paper, a comprehensive study on the electonic properties of hBN/graphene were executed by highly accurate first-principles many-body perturbation theory approach. To exploit the potential of the hBN/graphene its electronic properties at interlayer distance from 1.5 to 3.5 Å were studied. The calculated G0W0 band gap of hBN sheet was found to be 6.09 eV and this value is in good agreement with experimental value of 6 eV. For the heterostructure, the calculated band gaps of hBN/graphene by varying the interlayer distance from 1.5 to 3.5 Å was found to be 1.76, 1.70, 0.84, 0.22 0.04 eV for interlayer distance of 1.5, 2.0, 2.5, 3.0 and 3.5 eV. The energy analysis of hBN/graphene heterostructure reveal that the most stable configuration is the one in which the either B or N atom of hBN facing to graphene is above the hole center of graphene. The calculated optical gap of 6.0 eV for pure hBN sheet is in good agreement with experimental value. For hBN/graphene sheet the optical gap which correspond to the quasiparticle band gap was found to be 1.7 eV at interlayer distance of 2.0 Å. Conparing the optical absoption spectra, absorption in hBN/graphene is almost eight times that of pure hBN sheet. Optical gap of 1.7 eV and strong absorption within visible light waveleghts in hBN/graphene sheets suggest that the heterostruture consider in this paper is a promising candidate for solar cells applications.

Declarations

Ethics approval and consent to participate

Not Applicable.

Consent for publication

All authors have read and consented to the submission of the manuscript.

Availability of data and material

Not Applicable.

Competing interests

All authors declare no competing interests.

Acknowledgment

The authors are grateful to the reviewers for valuable comments and thoughtful observations.

References

Aga, G. S., Singh, P., & Geffe, C. A. (2023). First-Principles Study of the Quasi-Particle and Excitonic Effect in o-BC2N: The GW+ BSE Study. Advances in Condensed Matter Physics, 2023(1), 7808434.

Ahmed, M. S., Begum, H., Kim, Y.-B., & Jung, S. (2021). Surface functionalization of acidified graphene through amidation for enhanced oxygen reduction reaction. Applied Surface Science, 536, 147760.

Chen, H.-T., Padilla, W. J., Zide, J. M., Gossard, A. C., Taylor, A. J., & Averitt, R. D. (2006). Active terahertz metamaterial devices. Nature, 444(7119), 597-600.

Dal Corso, A., Baroni, S., Resta, R., & de Gironcoli, S. (1993). Ab initio calculation of phonon dispersions in II-VI semiconductors. Physical Review B, 47(7), 3588.

Das, S., Pandey, D., Thomas, J., & Roy, T. (2019). The role of graphene and other 2D materials in solar photovoltaics. Advanced Materials, 31(1), 1802722.

Ersan, G., Apul, O. G., Perreault, F., & Karanfil, T. (2017). Adsorption of organic contaminants by graphene nanosheets: A review. Water research, 126, 385-398.

Escudero, D., Duchemin, I., Blase, X., & Jacquemin, D. (2017). Modeling the Photochrome–TiO2 Interface with Bethe–Salpeter and Time-Dependent Density Functional Theory Methods. The journal of physical chemistry letters, 8(5), 936-940.

Giannozzi, P., Baroni, S., Bonini, N., Calandra, M., Car, R., Cavazzoni, C., Dabo, I. (2009). QUANTUM ESPRESSO: a modular and open-source software project for quantum simulations of

materials. Journal of physics: Condensed matter, 21(39), 395502.

Godby, R., & Needs, R. (1989a). Metal-insulator transition in Kohn-Sham theory and quasiparticle theory. Physical review letters, 62(10), 1169.

Godby, R., & Needs, R. (1989b). The metal-insulator transition in quasiparticle theory and Kohn-Sham theory. Physical review letters, 62(10), 1169-1172.

Harsha, G., Abraham, V., Wen, M., & Zgid, D. (2024). Quasiparticle and fully self-consistent GW methods: an unbiased analysis using Gaussian orbitals. arXiv preprint arXiv:2406.18077.

Huang, B., & Lee, H. (2012). Defect and impurity properties of hexagonal boron nitride: A first-principles calculation. Physical Review B, 86(24), 245406.

Huang, X., Guan, J., Lin, Z., Liu, B., Xing, S., Wang, W., & Guo, J. (2017). Epitaxial growth and band structure of Te film on graphene. Nano letters, 17(8), 4619-4623.

Hybertsen, M. S., & Louie, S. G. (1984). Non-local density functional theory for the electronic and structural properties of semiconductors. Solid State Communications, 51(7), 451-454.

Idris, B., Lawal, A., Abubakar, D., & Dalhatu, S. A. (2021). Ab initio Calculation of CuSbSe2 in Bulk and Monolayer for Solar Cell and Infrared Optoelectronic Applications. Communication in Physical Sciences, 7(3).

Idris, M., Shaari, A., Razali, R., Lawal, A., & Ahams, S. (2020). DFT+ U studies of structure and optoelectronic properties of Fe2SiO4 spinel. Computational Condensed Matter, 23, e00460.

Itas, Y. S., Razali, R., Tata, S., Kolo, M., Lawal, A., Alrub, S. A., Khandaker, M. U. (2023). DFT Studies on the Effects of C Vacancy on the CO2 Capture Mechanism of Silicon Carbide Nanotubes Photocatalyst (Si12C12-X; X= 1; 2). Silicon, 1-11.

Itas, Y. S., Suleiman, A. B., Ndikilar, C. E., Lawal, A., Razali, R., Khandaker, M. U., Idris, A. M. (2023). New trends in the hydrogen energy storage potentials of (8, 8) SWCNT and SWBNNT using optical adsorption spectra analysis: a DFT study. Journal of Computational Electronics, 22(6), 1595-1605.

Itas, Y. S., Suleiman, A. B., Ndikilar, C. E., Lawal, A., Razali, R., Ullah, M. H., Khandaker, M. U. (2023). DFT Studies of the Photocatalytic Properties of MoS2-Doped Boron Nitride Nanotubes for Hydrogen Production. ACS Omega.

Jariwala, D., Srivastava, A., & Ajayan, P. M. (2011). Graphene synthesis and band gap opening. Journal of nanoscience and nanotechnology, 11(8), 6621-6641.

Körbel, S., Kammerlander, D., Sarmiento-Pérez, R., Attaccalite, C., Marques, M. A., & Botti, S. (2016). Publisher's Note: Optical properties of Cu-chalcogenide photovoltaic absorbers from self-consistent G W and the Bethe-Salpeter equation [Phys. Rev. B 91, 075134 (2015). Physical Review B, 93(15), 159901.

Lawal, A. (2017). Theoretical Study of Structural, Electronic and Optical Properties of Bismuth-Selenide, Bismuth-Telluride and Antimony-Telluride/Graphene Heterostructure for Broadband Photodetector, Universiti Teknologi Malaysia.

Lawal, A., Bello, M., & Kona, A. M. (2022). Quasi-particle band structure and optical properties of Perylene Crystal for Solar Cell Application: A G0W0 Calculations. Communication in Physical Sciences, 8(2).

Lawal, A., Shaari, A., Ahmed, R., & Jarkoni, N. (2017a). First-principles many-body comparative study of Bi2Se3 crystal: A promising candidate for broadband photodetector. Physics Letters A, 381(35), 2993-2999.

Lawal, A., Shaari, A., Ahmed, R., & Jarkoni, N. (2017b). Sb2Te3 crystal a potential absorber material for broadband photodetector: A first-principles study. Results in physics, 7, 2302-2310.

Lawal, A., Shaari, A., Ahmed, R., Taura, L., Madugu, L., & Idris, M. (2019). Sb2Te3/graphene heterostructure for broadband photodetector: A first-principles calculation at the level of Cooper's exchange functionals. Optik, 177, 83-92.

Lawal, A., Taura, L., Abdullahi, Y. Z., Shaari, A., Suleiman, A. B., Gidado, A., & Chiromawa, I. M. (2022). Corrections of band gaps and optical spectra of N-doped Sb2Se3 from G0W0 and BSE calculations. Physics B: Condensed Matter, 646, 414307.

Liu, H., Xi, P., Xie, G., Shi, Y., Hou, F., Huang, L., Wang, J. (2012). Simultaneous reduction and surface functionalization of graphene oxide for hydroxyapatite mineralization. The Journal of Physical Chemistry C, 116(5), 3334-3341.

Liu, X., Chao, D., Su, D., Liu, S., Chen, L., Chi, C., Mai, L. (2017). Graphene nanowires anchored to 3D graphene foam via self-assembly for high performance Li and Na ion storage. Nano Energy, 37, 108-117.

Luo, X., Sullivan, M. B., & Quek, S. Y. (2012). First-principles investigations of the atomic, electronic, and thermoelectric properties of equilibrium and strained Bi 2 Se 3 and Bi 2 Te

3 including van der Waals interactions. Physical Review B, 86(18), 184111.

Margine, E. R., Bocquet, M. L., & Blase, X. (2008). Thermal Stability of Graphene and Nanotube Covalent Functionalization doi: 10.1021/nl801718f]. Nano Letters, 8(10), 3315-3319. https://doi.org/10.1021/nl801718f.

Marini, A., Hogan, C., Grüning, M., & Varsano, D. (2009). Yambo: an ab initio tool for excited state calculations. Computer Physics Communications, 180(8), 1392-1403.

Medeiros, P. V., Stafström, S., & Björk, J. (2014). Effects of extrinsic and intrinsic perturbations on the electronic structure of graphene: Retaining an effective primitive cell band structure by band unfolding. Physical Review B, 89(4), 041407.

Mondal, W. R., & Pati, S. K. (2012). A study on the surface states of a topological insulator: Bi2Se3. arXiv preprint arXiv:1208.1482.

Monkhorst, H. J., & Pack, J. D. (1976). Special points for Brillouin-zone integrations. Physical Review B, 13(12), 5188.

Novoselov, K. S., Geim, A. K., Morozov, S. V., Jiang, D.-e., Zhang, Y., Dubonos, S. V., Firsov, A. A. (2004). Electric field effect in atomically thin carbon films. Science, 306(5696), 666-669.

Quílez-Bermejo, J., Morallón, E., & Cazorla-Amorós, D. (2020). Metal-free heteroatom-doped carbon-based catalysts for ORR: A critical assessment about the role of heteroatoms. Carbon, 165, 434-454.

Radzwan, A., Ahmed, R., Shaari, A., Ng, Y. X., & Lawal, A. (2018). First-principles calculations of the stibnite at the level of modified Becke–Johnson exchange potential. Chinese journal of physics, 56(3), 1331-1344.

Rohlfing, M., & Louie, S. G. (2000). Electron-hole excitations and optical spectra from first principles. Physical Review B, 62(8), 4927.

Santra, S., Ghosh, A., Das, B., Pal, S., Pal, S., & Adalder, A. (2024). Beyond the horizons of graphene: xenes for energy applications. RSC Sustainability, 2(6), 1631-1674.

Shi, Y., Hamsen, C., Jia, X., Kim, K. K., Reina, A., Hofmann, M., Juang, Z.-Y. (2010). Synthesis of few-layer hexagonal boron nitride thin film by chemical vapor deposition. Nano letters, 10(10), 4134-4139.

Solozhenko, V., Lazarenko, A., Petitet, J.-P., & Kanaev, A. (2001). Bandgap energy of graphite-like hexagonal boron nitride. Journal of Physics and Chemistry of Solids, 62(7), 1331-1334.

Song, L., Ci, L., Lu, H., Sorokin, P. B., Jin, C., Ni, J., Yakobson, B. I. (2010). Large scale growth and characterization of atomic hexagonal boron nitride layers. Nano letters, 10(8), 3209-3215.

Wang, H. S., Chen, L., Elibol, K., He, L., Wang, H., Chen, C., Cong, C. X. (2021). Towards chirality control of graphene nanoribbons embedded in hexagonal boron nitride. Nature Materials, 20(2), 202-207.

Wang, N., Yang, G., Wang, H., Yan, C., Sun, R., & Wong, C.-P. (2019). A universal method for large-yield and high-concentration exfoliation of two-dimensional hexagonal boron nitride nanosheets. Materials Today, 27, 33-42.

Watanabe, K., Taniguchi, T., & Kanda, H. (2004). Direct-bandgap properties and evidence for ultraviolet lasing of hexagonal boron nitride single crystal. Nature Materials, 3(6), 404-409.

Xu, S., Al Ezzi, M. M., Balakrishnan, N., Garcia-Ruiz, A., Tsim, B., Mullan, C.Taniguchi, T. (2021). Tunable van Hove singularities and correlated states in twisted monolayer–bilayer graphene. Nature Physics, 17(5), 619-626.

Yang, Y., Ma, J., Yang, J., & Zhang, Y. (2024). Graphene/h-BN hybrid van der Waals structures with high strength and flexibility: A nanoindentation investigation. Thin-Walled Structures, 195, 111341.

Yusuf, I. D., Suleiman, A. B., Lawal, A., Ndikilar, C. E., Taura, L., Gidado, A., & Chiromawa, I. M. (2024). Significant improvement in structural, electronic, optical and thermoelectric properties of PdTe2 in bulk and monolayer phase: A G0W0+ BSE approach. Physica B: Condensed Matter, 685, 416015.

Zhao, Y., Wu, X., Yang, J., & Zeng, X. C. (2012). Oxidation of a two-dimensional hexagonal boron nitride monolayer: a first-principles study. Physical Chemistry Chemical Physics, 14(16), 5545-5550.